Classical dynamics of a non-integrable Hamiltonian near coupling-induced resonance islands

1996 J. Phys. A: Math. Gen. 29 5963

(http://iopscience.iop.org/0305-4470/29/18/025)

J. Phys. A: Math. Gen. **29** (1996) 5963–5977. Printed in the UK

Classical dynamics of a non-integrable Hamiltonian near coupling-induced resonance islands

Marc Joyeux

Laboratoire de Spectrométrie Physique (CNRS UA08), Université Joseph Fourier-Grenoble I, BP87, 38402 St Martin d'Hères Cedex, France

Received 14 December 1995, in final form 31 May 1996

Abstract. The purpose of this article is the description of the classical dynamics of a resonant non-integrable Hamiltonian, which is written in the form

$$H = \omega_1 I_1 + \omega_2 I_2 + x_{11} I_1^2 + x_{22} I_2^2 + x_{12} I_1 I_2 + 2k_{mn} I_1^{m/2} I_2^{n/2} \cos(m\varphi_1 - n\varphi_2) + k_C I_1^{a/2} I_2^{b/2} \cos(r\varphi_1 + s\varphi_2)$$

and where the term with k_C behaves as a perturbation to the remaining integrable part (call it H_F) of the Hamiltonian. Apart from the chaotic region around the separatrix of H_F, the dynamics of H is clearly different from that of H_F only in the neighbourhood of low-order periodic orbits of H_F, where coupling-induced resonance islands are seen to emerge. In order to model these resonance islands, H_F is Taylor expanded in terms of its action integrals (thanks to recent exact analytical calculations) and the perturbation with k_C is Fourier expanded in terms of the angles conjugate to the actions of H_F. Retaining in the expansion only the term which is almost secular (because of the vicinity of the periodic orbit) leads to a local single resonance form of H. The classical frequencies and action integrals, which can be calculated analytically for this local expression of H, are shown to be in excellent agreement with 'exact' numerical values deduced from power spectra and Poincaré surfaces of section. It is pointed out in the discussion that all the trajectories inside coupling-induced resonance islands share one almost degenerate classical frequency, and that the width of the coupling-induced island grows as the square root of the perturbation parameter k_C, but is inversely proportional to the square root of the slow classical frequency at the periodic orbit and to the square root of the derivative, with respect to the first action integral, of the winding number.

1. Introduction

Let us first consider the 2D Dunham expansion Hamiltonian

$$H_D(I_1, I_2, \varphi_1, \varphi_2) = \omega_1 I_1 + \omega_2 I_2 + x_{11} I_1^2 + x_{22} I_2^2 + x_{12} I_1 I_2 \tag{1.1}$$

where the momentum coordinate I_i is conjugate to the position coordinate φ_i. This kind of Hamiltonian (with three degrees of freedom instead of only two and with anharmonicity parameters with degree higher than two) accurately describes some 'simple' molecules as NO_2 (up to the conical intersection at about 10 000 cm^{-1} vibrational energy) [1–3] or SO_2 [4] (for the whole range of recorded spectra, that is up to 20 000 cm^{-1} vibrational energy). The classical dynamics of this Hamiltonian is trivial: since the expression of H_D does not depend on the φ_i's, I_1 and I_2 are the action integrals of the system and their conjugate angles evolve linearly with time, according to $\varphi_1 = (\omega_1 + 2x_{11}I_1 + x_{12}I_2)t$ and $\varphi_2 = (\omega_2 + 2x_{22}I_2 + x_{12}I_1)t$. The whole phase space is regular (non-chaotic).

0305-4470/96/185963+15$19.50

Let us now add to H_D a first term depending on the zero-order angles φ_i:

$$H_F(I_1, I_2, \varphi_1, \varphi_2) = H_D(I_1, I_2, \varphi_1, \varphi_2) + 2k_{mn} I_1^{m/2} I_2^{n/2} \cos(m\varphi_1 - n\varphi_2). \tag{1.2}$$

The additional term in equation (1.2) has not been chosen at random: it is that one, which is obtained when applying perturbation theories, such as secular perturbation theory or Birkhoff–Gustavson perturbation theory [5–8], to a Hamiltonian with a polynomial expansion of the potential energy. As a consequence, the Hamiltonian in equation (1.2) is precisely the one which is used by spectroscopists to fit the vibrational spectra of molecules with two modes in near m:n resonance, such as for instance CS_2 (m:n = 1:2) [9–12]. The resonance Hamiltonian in equation (1.2) has also been used to study many other problems of interest in molecular physics, such as, for example, the energy transfer between bonds in triatomic molecules [13, 14], the normal to local transition in coupled vibrations [15, 16], the semiclassical quantization of strongly resonant systems [7, 9, 17–20], the semiclassical theory of avoided crossings and of the related dynamical tunnelling [8, 21, 22], the influence of classical resonances on quantum energy levels [23], the periodic orbit description of the Fourier transform of molecular spectra [24] and the application of Berry and Tabor's trace formula to a Hamiltonian of spectroscopic interest [25]. The Hamiltonian H_F is still integrable, since $I = nI_1 + mI_2$ and the energy E are two constants of the motion. It has been shown recently, that Hamilton's equations can be solved exactly and analytically for the fundamental m:n = 1:1, 1:2 and 1:3 resonances, leading to simple expressions for the fundamental frequencies of the tori supporting the trajectories and for the corresponding action integrals [17, 26].

A natural development consists in adding to H_F a second term which depends on the angles φ_i's. The Hamiltonian is thus expressed in the form

$$\begin{aligned} H &\equiv E = H_F(I_1, I_2, \varphi_1, \varphi_2) + k_C H_C(I_1, I_2, \varphi_1, \varphi_2) \\ H_C(I_1, I_2, \varphi_1, \varphi_2) &= I_1^{a/2} I_2^{b/2} \cos(r\varphi_1 + s\varphi_2). \end{aligned} \tag{1.3}$$

This Hamiltonian can be thought of as describing the vibrations of a molecule in the region where the single resonance approximation first becomes insufficient. Alternatively, it can be understood as resulting from the Birkhoff–Gustavson perturbation theory [5–8] applied to a polynomial potential when a second angle $r\varphi_1 + s\varphi_2$ is added to the so-called null-space. Such a Hamiltonian has been used, for instance, to study the amplitude instability and ergodic behaviour for conservative nonlinear oscillator systems [27], the influence of resonance overlapping on the emergence of chaotic motion [28, 29], the intramolecular energy redistribution in centrosymmetric chains [30] and the quantum analysis of the transition towards vibrational chaos in triatomic molecules [31].

The major difference between H and H_F arises from the fact that $I = nI_1 + mI_2$ no longer remains constant and that chaotic motion can occur. The Hamiltonian H in equation (1.3) is actually an example of an intermediate regime well described by the KAM (Kolmogorov–Arnold–Moser) theorem [32–36]: for low values of k_C, rational tori are destroyed but most trajectories on irrational tori remain regular, whereas for larger values of k_C an increasing macroscopic portion of the phase space is invaded by chaotic trajectories. The interesting feature of H is that the amount of non-integrability continuously increases with increasing values of k_C, whereas the evolution towards chaos is rather more complex for seemingly simpler Hamiltonians like the polynomial potential.

The purpose of the present paper is to provide analytical results for the understanding of the dynamics (classical frequencies, action integrals and phase space structure) of the non-integrable Hamiltonian H in the regions where this study can still be performed, that is outside chaotic regions. A first, physical, application of these calculations deals with

the assignment of individual levels in the vibrational spectra of molecules whenever a polynomial expression is known for the potential energy surface. This polynomial expression might have been obtained either from the fit of observed levels or from *ab initio* calculations. As stated a few lines above, addition of a second angle in the null-space of the Birkhoff–Gustavson perturbation theory [5–8] leads locally to the Hamiltonian H in equation (1.3), which is a better approximation than the single resonance approximation in equation (1.2) or the diagonal expansion in equation (1.1). The two action integrals, which are calculated for H, are approximate constants of the motion for the full polynomial Hamiltonian and can be used through Einstein–Brillouin–Keller (EBK) semiclassical quantization to label quantum levels. A second possible application of these calculations deals with the semiclassical trace formula, which has been derived by Ozorio de Almeida for mixed systems [37] and has been further discussed by Tomsovic *et al* [38]. This trace formula expresses the density of states as a function of the classical properties of the hyperbolic and elliptic fixed points, which result from the destruction of each rational torus. This paper should, therefore, enable an easy application of Ozorio de Almeida trace formula to all the Hamiltonians which can be locally approximated according to equation (1.3).

It is shown in section 2 that the classical dynamics of H is very close to that of H_F far from the coupling-induced resonance islands that develop around periodic orbits (POs) of H_F, but that great distortions occur in the neighbourhood and inside these islands. In order to enable further analytical calculations, a local single resonance form of H around POs of H_F is derived in section 3, using the solutions of Hamiltonian's equations obtained in [17, 26] for H_F. The expressions of the classical frequencies and of the action integrals of the local Hamiltonian are then given in section 4. Finally, the validity of the whole analytical procedure is checked in section 5 against 'exact' results deduced from power spectra and Poincaré surfaces of section and the results are discussed.

2. Coupling-induced resonance islands around POs of H_F

Using the usual canonical transformation, according to

$$I = nI_1 + mI_2 \qquad J = nI_1 \qquad \theta = \frac{\varphi_2}{m} \qquad \psi = \frac{\varphi_1}{n} - \frac{\varphi_2}{m} \tag{2.1}$$

the Hamiltonian H in equation (1.3) is rewritten in the form

$$\begin{aligned} H &\equiv E = H_F(I, J, \theta, \psi) + K_C H_C(I, J, \theta, \psi) \\ H_F(I, J, \theta, \psi) &= \omega I + \varepsilon J + \chi_I I^2 + \chi_J J^2 + \chi_{IJ} IJ + K J^{m/2}(I - J)^{n/2} \cos(mn\psi) \\ H_C(I, J, \theta, \psi) &= J^{a/2}(I - J)^{b/2} \cos((rn + sm)\theta + rn\psi) \end{aligned} \tag{2.2}$$

with the following relations between the old and new parameters:

$$\begin{aligned} &\omega = \frac{\omega_2}{m} \qquad \varepsilon = \frac{\omega_1}{n} - \frac{\omega_2}{m} \qquad K = \frac{2k_{mn}}{n^{m/2}m^{n/2}} \qquad K_C = \frac{k_C}{n^{a/2}m^{b/2}} \\ &\chi_I = \frac{x_{22}}{m^2} \qquad \chi_J = \frac{x_{11}}{n^2} - \frac{x_{12}}{mn} + \frac{x_{22}}{m^2} \qquad \chi_{IJ} = \frac{x_{12}}{mn} - 2\frac{x_{22}}{m^2}. \end{aligned} \tag{2.3}$$

The explicit Hamiltonian which will be used throughout this paper for the purpose of illustration is

$$\begin{aligned} H(I_1, I_2, \varphi_1, \varphi_2) \equiv E &= \omega_1 I_1 + \omega_2 I_2 + x_{11} I_1^2 + x_{22} I_2^2 + x_{12} I_1 I_2 \\ &\quad + 2k_{mn}\sqrt{I_1} I_2 \cos(\varphi_1 - 2\varphi_2) + k_C I_2^2 \cos(2\varphi_2) \end{aligned} \tag{2.4}$$

that is $m = 1$, $n = 2$, $a = 0$, $b = 4$, $r = 0$ and $s = 2$ in equations (1.2) and (1.3). The choice for the parameters a, b, r and s is unimportant, because, as will be developed in section 3,

H_C is dealt with using perturbative schemes anyway. In contrast, the method used in this paper is restricted to values of m:n equal to 1:1, 1:2, 1:3 and 2:2, because the analytical solutions of Hamilton's equations for H_F were found only for these fundamental resonances [17, 26]. To my knowledge, no analytical solution can be given for Hamilton's equations dealing with H_F for values of m and n such that $m + n > 4$, so that much more drastic approximations must be made to study the classical dynamics of the Hamiltonian H with two angle-dependent terms. For instance, one can replace in H_F the term $2k_{mn}I_1^{m/2}I_2^{n/2}$ by some average value, which is either taken at random or estimated from plots (as in [8, 18]), and then proceed along the same lines as here. One interesting point in the cases with $m+n \leqslant 4$ is that it requires no approximation for H_F and no numerical plot, except for the sake of comparison. The following numerical values of the spectroscopic parameters are used:

$$\begin{aligned} &\omega_1 = 2 \qquad \omega_2 = \sqrt{5} - 1 \qquad k_{12} = -0.1000 \qquad k_C = -0.0004 \\ &x_{11} = -0.0060 \qquad x_{22} = 0.0010 \qquad x_{12} = -0.0025. \end{aligned} \tag{2.5}$$

The expression of the Hamiltonian in equation (2.4) in terms of the (I, J, θ, ψ) set of coordinates is

$$\begin{aligned} H \equiv E = \omega I + \varepsilon J + \chi_I I^2 + \chi_J J^2 + \chi_{IJ} I J + K\sqrt{J}(I - J)\cos(2\psi) \\ + K_C(I - J)^2 \cos(2\theta). \end{aligned} \tag{2.6}$$

An example of (I, θ) and (J, ψ) Poincaré surfaces of section drawn at energy $E = 15$ for the complete Hamiltonian H in equation (2.6) is given in figure 1. Two major differences are pointed out when comparing this figure with that obtained for the integrable case with $K_C = 0$ (see for instance [17]). The most striking one is obviously the region almost ergodically filled with points, which is associated with chaotic motion around the hyperbolic fixed point separatix of H_F. In that region trajectories do not remain on a 2D torus defined by two action integrals, but instead explore a 3D subspace of the complete 4D phase space. Study of this region is not within the scope of the present paper (see, however, the end of section 5). Outside from the chaotic region almost all the phase space is occupied by regular trajectories, which are more or less distorted compared to the integrable case. As will become clearer later, the most distorted trajectories are to be found around those values of I which correspond to low rational values of the ratio of the classical frequencies of the integrable Hamiltonian H_F (ω^*/ν^* equal to $\frac{2}{1}, \frac{1}{1}, \frac{1}{2}, \frac{1}{3}, \frac{2}{3}, \ldots$, where ω^* and ν^* denote the two classical frequencies of H_F, as in [17, 26]). Near these periodic orbits (POs), the trajectories brake into resonance islands. In order not to confuse these resonance islands with resonant trajectories of H_F, they will hereafter be called the 'coupling-induced' resonance islands. For instance, circled in figure 1 are the coupling-induced resonance islands, which develop around the $\omega^*/\nu^* = \frac{2}{3}$ PO of H_F with first action integral $I_{PO} \approx 14.270\,25$. The resonance islands around the $\omega^*/\nu^* = \frac{1}{2}$ PO of H_F with first action integral $I_{PO} \approx 15.148\,27$ are also clearly seen quite near to the chaotic region.

The purpose of the present paper is to study the classical dynamics of the non-integrable Hamiltonian H near these coupling-induced resonance islands. Indeed, the classical dynamics of H away from these islands is not very different from the dynamics of the integrable Hamiltonian H_F, which has already been thoroughly investigated [17, 26]. As an example, the classical frequencies of H deduced from the plot of the power spectra are reported in figure 2 for initial values of I ranging from $I_0 = 12.83$–13.68, that is far enough from the $\frac{2}{3}$ PO. The classical frequencies of H_F, which are calculated according to [17, 26], are plotted on the same figure. The excellent agreement between the two plots shows that H_C can freely be neglected away from coupling-induced resonance islands, at least

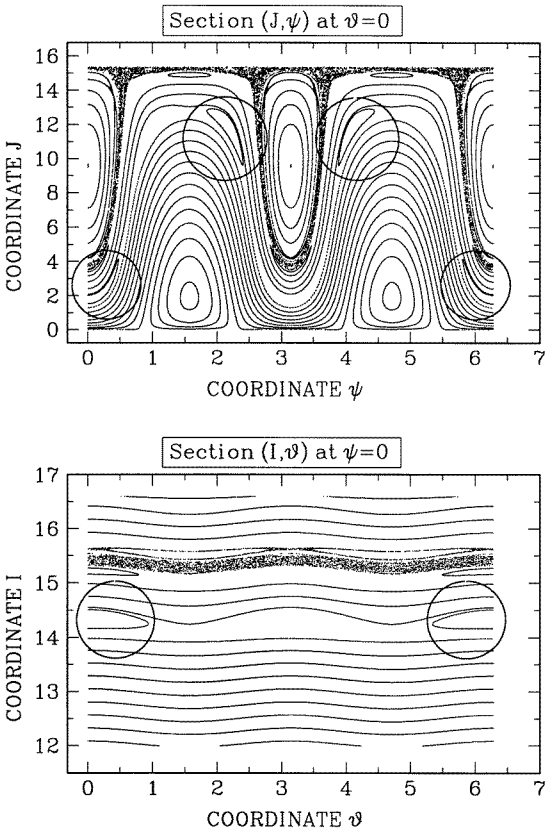

Figure 1. Poincaré surfaces of section (SOS) drawn for the full, non-integrable Hamiltonian H at energy $E = 15$. The (J, ψ) SOS at $\theta = 0$ (modulo 2π) contains 33 trajectories with initial values of I ranging from $I_0 = 11.065$ to $I_0 = 16.585$ with increments of 0.24. Trajectories with the lowest values of I_0 are those circling around the elliptic fixed points on the $\psi = \pi/2$ and $\psi = 3\pi/2$ axes, whereas trajectories with the highest values of I_0 are those circling around the elliptic fixed points on the $\psi = 0$ (or 2π) and $\psi = \pi$ axes. The initial value of θ is $\theta_0 = \pi/4$ and the initial value of ψ is $\psi_0 = 0$ for non-resonant trajectories and $\psi_0 = k\pi/2$ ($k = 0, 1, 2, 3$) for resonant trajectories winding around an elliptic fixed point on the $\psi = k\pi/2$ axis. The (I, θ) SOS at $\psi = 0$ (modulo 2π) contains 20 trajectories with values of I_0 ranging from 12.025 to $I_0 = 16.585$ with increments of 0.24. The resonant trajectories with initial values of I_0 equal to 11.065, 11.305, 11.545 and 11.785, which are drawn for the (J, ψ) SOS, never cut the $\psi = 0$ surface. Initial values of θ and ψ are, $\theta_0 = \pi/4$ and $\psi_0 = 0$ respectively. At $K_C = 0$, the phase space is completely described by the values of I at the elliptic fixed points ($I_{min} \approx 11.015\,242$ and $I_{max} \approx 16.585\,125$) and at the hyperbolic fixed point separatrix ($I^+ \approx 15.353\,599$) and by that value of I, which separates resonant from non-resonant trajectories without being associated with any fixed point ($I^- \approx 12.018\,399$) [26]. The chaotic trajectory, which is clearly seen in both SOS, has initial value $I_0 = 15.385$. The circles surround the coupling-induced resonance islands, which are the traces of the trajectory with initial value $I_0 = 14.185$. Other coupling-induced resonance islands with initial value $I_0 = 15.145$ ($\frac{1}{2}$ PO of H_F) can be seen close to the chaotic trajectory.

up to a given accuracy. As can be seen in figure 3, this is no longer the case for values of I_0 ranging from 13.83 to 14.68, that is, those values which surround the first action integral $I_{PO} \approx 14.270\,25$ of the $\frac{2}{3}$ PO of H_F. The large discrepancies observed in figure 3 between the calculated classical frequencies of H_F and the observed classical frequencies

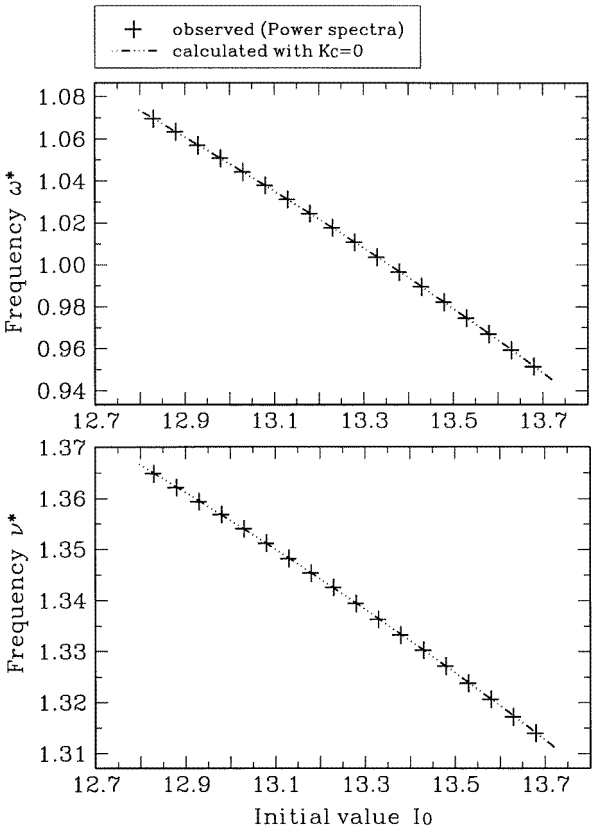

Figure 2. Plot of the classical frequencies ω^* and ν^* for initial values of I ranging from $I_0 = 12.83$ to $I_0 = 13.68$ (that is, far enough from the $\frac{2}{3}$ PO of H_F) for the non-integrable Hamiltonian H at energy $E = 15$. Other initial values are $\psi_0 = 0$ and $\theta_0 = \pi/4$ (see text). The dot-dashed line corresponds to the classical frequencies of H_F calculated according to the formula in [17, 26]. The exact classical frequencies for the non-integrable Hamiltonian H are deduced from power spectra obtained from numerical integration of trajectories for a time $\Delta t = 30\,000$. The absolute precision for observed classical frequencies is about 10^{-4}.

of H clearly demonstrate that additional studies are needed in the neighbourhood of these coupling-induced resonance islands.

3. Derivation of a local single resonance form of H around POs of H_F

One method to obtain a simpler, analytically treatable form of H near a PO of H_F consists of (i) Taylor expanding H_F to second order as a function of its classical action integrals I and $\mathcal{I}_2$, (ii) Fourier expanding H_C as a function of the two angles V and Ω, conjugate respectively to I and $\mathcal{I}_2$, (iii) retaining in the Fourier expansion of H_C only the term which is almost secular because of the neighbourhood of the PO. One is then led to a local single resonance Hamiltonian with a constant prefactor for the cosine term.

But, first of all, let us review very briefly the classical mechanics of the Hamiltonian H_F for the $m{:}n = 1{:}1$, 1:2 and 1:3 resonances. Since the expression of H_F in equation (2.2)

does not depend on θ, I is a consatnt of the motion for the Hamiltonian H_F. Hamilton's equations for the three other coordinates can be solved analytically and the solutions can be put in the form

$$\begin{aligned} J(t) &= F(\omega^* t - \Delta_0) \\ \psi(t) &= \psi_0 + z\omega^* t + G(\omega^* t) \\ \theta(t) &= \theta_0 + \nu^* t + H(\omega^* t) \end{aligned} \tag{3.1}$$

where F, G and H are three periodic functions with period 2π. F is an even function, whereas G and H are odd functions, which satisfy $G(0) = H(0) = 0$. ψ_0 and θ_0 are the values of ψ and θ at time $t = 0$, whereas Δ_0 is a phase shift, which depends on the value J_0 of J at $t = 0$. It is most important in equation (3.1) to use the equations in [26], which take into account initial values, rather than those in [17], which do not take into account initial values. ω^* and ν^* are the two fundamental frequencies of the tori supporting the trajectories. z is a phase space structure parameter, which is equal to zero for resonant trajectories of H_F and to $\pm 1/n$ for non-resonant trajectories of H_F. The first action integral of the system is just I. The second action integral of the system is labelled $\mathcal{I}_2$. Its expression is also to be found in [17, 26]. The angles conjugate to the actions I and $\mathcal{I}_2$ are $V = \nu^* t$ and $\Omega = \omega^* t$, respectively. Note that at time $t = 0$, one has $V(0) = \Omega(0) = 0$.

Let us now consider one trajectory of the non-separable Hamiltonian H in equation (2.2) with initial values $(I_0, J_0, \theta_0, \psi_0)$ at time $t = 0$. Taylor expansion of the energy in the neighbourhood of the trajectory of H_F with action integrals I_0 and $\mathcal{I}_{20}$ and energy E leads to

$$\begin{aligned} E' &= \omega_1' I + \omega_2' \mathcal{I}_2 + x_{11}' I^2 + x_{22}' \mathcal{I}_2^2 + x_{12}' I \mathcal{I}_2 + \cdots + K_C H_C \\ x_{11}' &= \frac{1}{2}\nu_0^* \left(\frac{\partial \nu^*}{\partial E}\right)_0 + \frac{1}{2}\left(\frac{\partial \nu^*}{\partial I}\right)_0 \qquad x_{22}' = \frac{1}{2}\omega_0^* \left(\frac{\partial \omega^*}{\partial E}\right)_0 \qquad x_{12}' = \omega_0^* \left(\frac{\partial \nu^*}{\partial E}\right)_0 \\ \omega_1' &= \nu_0^* - 2x_{11}' I_0 - x_{12}' \mathcal{I}_{20} \qquad \omega_2' = \omega_0^* - x_{12}' I_0 - 2x_{22}' \mathcal{I}_{20} \\ E' &= \nu_0^* I_0 + \omega_0^* \mathcal{I}_{20} - x_{11}' I_0^2 - x_{22}' \mathcal{I}_{20}^2 - x_{12}' I_0 \mathcal{I}_{20}. \end{aligned} \tag{3.2}$$

In equation (3.2), derivatives with respect to I are calculated at a constant value of the energy E (and not of the second action integral $\mathcal{I}_2$) and derivatives with respect to E at constant value of I. The 0 subscript means that the classical frequencies of $H_F(\nu^*, \omega^*)$ and their derivatives are taken at E and I_0. The additional term H_C is then treated as a perturbation and Fourier expanded as a function of the angles $V = \nu^* t$ and $\Omega = \omega^* t$ using equation (3.1). Calculations can be somewhat simplified by assuming that initial values are chosen such that $\Delta_0 = 0$ or $\Delta_0 = \pi$, which implies that $F(\Omega - \Delta_0)$ is an even function of Ω (and not just of $\Omega - \Delta_0$). One obtains

$$\begin{aligned} H_C &= \sum_{k=-\infty}^{+\infty} h_k \cos((rn + sm)V - k\Omega + \delta_0) \\ h_k &= \frac{1}{2\pi}\int_0^{2\pi} \mathrm{d}\Omega\, F(\Omega - \Delta_0)^{a/2} (I - F(\Omega - \Delta_0))^{b/2} \\ &\qquad \times \cos((rn + sm)H(\Omega) + rnG(\Omega) + (rnz + k)\Omega) \\ \delta_0 &= (rn + sm)\theta_0 + rn\psi_0. \end{aligned} \tag{3.3}$$

Around a particular PO, only the almost secular term $k = n'$ such that $(rn+sm)/n' \approx \nu^*/\omega^*$ is retained in equation (3.3). This leads to the expression of the local single resonance form

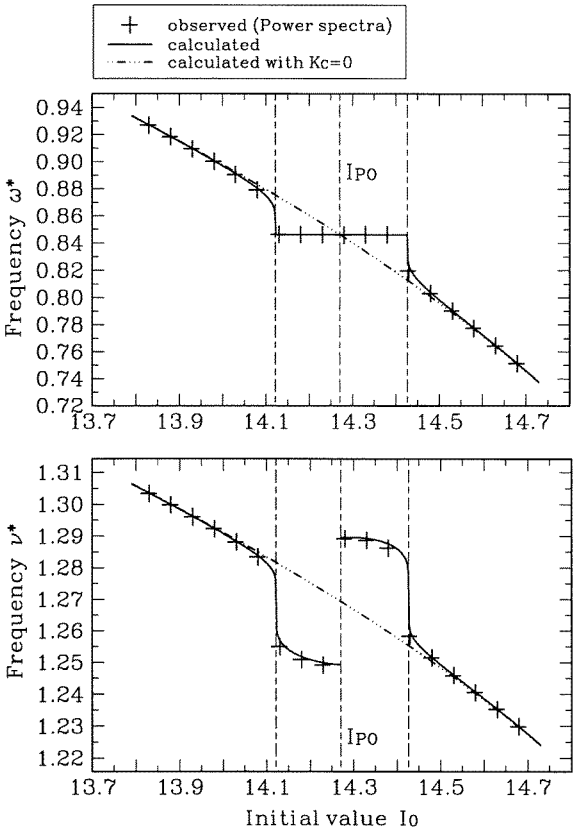

Figure 3. Plot of the classical frequencies ω^* and ν^* for initial values of I ranging from $I_0 = 13.83$ to $I_0 = 14.68$ (that is, surrounding the value $I_{\mathrm{PO}} \approx 14.270\,25$ of the first action integral of the $\frac{2}{3}$ PO of H_{F}) for the non-integrable Hamiltonian H at energy $E = 15$. Other initial values are $\psi_0 = 0$ and $\theta_0 = \pi/4$ (see text). The dot-dashed line corresponds to the classical frequencies of H_{F} calculated using the formula in [17, 26] and the full curve to the frequencies of H calculated according to equations (4.5), (4.6) and (5.3). The exact classical frequencies for the non-integrable Hamiltonian H are deduced from power spectra obtained from numerical integration of trajectories for a time $\Delta t = 30\,000$. The absolute precision for observed classical frequencies is about 10^{-4}.

of H:

$$E' \approx \omega'_1 I + \omega'_2 \mathcal{I}_2 + x'_{11} I^2 + x'_{22} \mathcal{I}_2^2 + x'_{12} I \mathcal{I}_2 + K' \cos(m'V - n'\Omega + \delta_0)$$
$$K' = K_c h_{n'} \qquad m' = rn + sm. \tag{3.4}$$

4. Classical dynamics of the local single resonance form of H

The classical dynamics of the local single resonance form of H in equation (3.4) is studied along the same lines as the dynamics of the resonance Hamiltonian H_{F} in equation (1.2) [17, 26]. The Hamiltonian is first rewritten according to the same canonical transformation as in equation (2.1):

$$I' = n'I + m'\mathcal{I}_2 \qquad J' = n'I \qquad \theta' = \Omega/m' \qquad \psi' = V/n' - \Omega/m' \tag{4.1}$$

where θ' is conjugate to I' and ψ' to J', leading to

$$E' = \omega' I' + \varepsilon' J' + \chi'_I I'^2 + \chi'_J J'^2 + \chi'_{IJ} I' J' + K' \cos(m' n' \psi' + \delta_0) \tag{4.2}$$

and relations similar to equation (2.3) between the old and new parameters:

$$\begin{aligned} &\omega' = \frac{\omega'_2}{m'} \qquad \varepsilon' = \frac{\omega'_1}{n'} - \frac{\omega'_2}{m'} \\ &\chi'_I = \frac{x'_{22}}{m'^2} \qquad \chi'_J = \frac{x'_{11}}{n'^2} - \frac{x'_{12}}{m'n'} + \frac{x'_{22}}{m'^2} \qquad \chi'_{IJ} = \frac{x'_{12}}{m'n'} - 2\frac{x'_{22}}{m'^2}. \end{aligned} \tag{4.3}$$

The Hamiltonian in equation (4.2) looks like that of the hindered rotor, which has been studied by several authors (see for instance [39, 40]). There, is however, a great difference, in the sense that the Hamiltonian in equation (4.2) is a Hamiltonian with two degrees of freedom, whereas the hindered rotor is a system with a single degree of freedom, and one must be careful not to loose one degree of freedom. The properties of the classical dynamics of the Hamiltonian in equation (4.2) can be sketched as follows. Since equation (4.2) does not depend on θ', I' is a constant of the motion. Let us define the constants A, B, C and R in terms of E' and I', according to

$$\begin{aligned} &A = (\varepsilon' + \chi'_{IJ} I')^2 + 4\chi'_J (E' - \omega' I' - \chi'_I I'^2) \\ &B = |4\chi'_J K'| \qquad C = -\varepsilon' - \chi'_{IJ} I' \qquad R = \frac{A+B}{2B}. \end{aligned} \tag{4.4}$$

Classical trajectories do not exist if $A < -B$. In contrast, a single librational trajectory is observed for each value of (E', I') if $|A| < B$, whereas two rotational trajectories coexist for each value of (E', I') if $A > B$. Librational trajectories correspond to trajectories inside coupling-induced resonance islands (resonant trajectories), whereas rotational trajectories lie outside the resonance islands (non-resonant trajectories). Librational/resonant trajectories are separated from rotational/non-resonant trajectories by two hyperbolic fixed point separatrices, which are defined by $A = B$ (that is $R = 1$). For librational/resonant trajectories ($|A| < B$), the classical frequencies $\nu^{*\prime}$ and $\omega^{*\prime}$ and the action integral $\mathcal{I}'_1$ and $\mathcal{I}'_2$ of the Hamiltonian in equation (4.2) are expressed in the form

$$\begin{aligned} &\omega^{*\prime} = \frac{m'n'G\pi\sqrt{2B}}{4K(R)} \qquad \nu^{*\prime} = G\left\{\omega' + 2\chi'_I I' + \frac{\chi'_{IJ}}{2\chi'_J} C\right\} \\ &\mathcal{I}'_1 = \frac{I'}{G} \qquad \mathcal{I}'_2 = \frac{2\sqrt{2B}}{m'n'G\pi\chi'_J}\{E(R) + (R-1)K(R)\} \end{aligned} \tag{4.5}$$

whereas for rotational/non-resonant trajectories ($A > B$)

$$\begin{aligned} &\omega^{*\prime} = \frac{n'G\pi\sqrt{A+B}}{2K(1/R)} \qquad \nu^{*\prime} = G\left\{\omega' + 2\chi'_I I' + \frac{\chi'_{IJ}}{2\chi'_J}\left(C \mp \frac{\omega^{*\prime}}{Gn'}\right)\right\} \\ &\mathcal{I}'_1 = \frac{I'}{G} \qquad \mathcal{I}'_2 = \frac{m'}{G\chi'_J}\left\{\mp\frac{C}{2} + \frac{\sqrt{A+B}}{\pi}E(1/R)\right\}. \end{aligned} \tag{4.6}$$

In equations (4.5) and (4.6), G denotes the greatest common divisor of m' and n' and arises, as well as the factor m' in the expression of $\mathcal{I}'_2$ for rotational trajectories, from the fact that action integrals must be calculated over closed loops gone through only once. The two rotational trajectories are characterized by opposite signs in the expressions of $\nu^{*\prime}$ and $\mathcal{I}'_2$. On the other hand, $\omega^{*\prime}$ vanishes at the separatices between librational and rotational trajectories, so that $\omega^{*\prime}$ and $\nu^{*\prime}$ continuously cross these separatrices, but each one with a vertical tangent (see figure 5 later).

5. Results and discussion

In order to use the formalism developed in sections 3 and 4 above, there only remains to determine how I' in equation (4.1) must be calculated. Indeed, I and $\mathcal{I}_2$ vary in time for the Hamiltonian H, and one is able to calculate analytically $\mathcal{I}_2$ for H_F but not for H. This problem can be solved by calculating $\mathcal{I}_2$ using the standard formula for the Hamiltonian H_F [17, 26] at a point where no energy is put in H_C, that is where the total phase $m'V - n'\Omega + \delta_0$ in equation (3.4) is equal to $(2k+1)\pi/2$. This can be done by checking for the phase while integrating trajectories numerically and calculating $\mathcal{I}_2$ and I' for the value of I which is arrived at the first time the phase crosses an odd multiple of $\pi/2$. However, a much simpler solution, which enables all the calculations to be performed analytically and avoids numerical integration of trajectories, consists of choosing initial values $(I_0, J_0, \theta_0, \psi_0)$ such that the phase at $t = 0$, that is δ_0, is precisely equal to an odd multiple of $\pi/2$. Then one just has

$$I' = n'I_0 + m'\mathcal{I}_{20}. \tag{5.1}$$

For the Hamiltonian in equation (2.6), the initial values $\theta_0 = \pi/4$ and $\psi_0 = 0$ satisfy both the condition on Δ_0 mentioned in section 3 (here $\Delta_0 = \pi$) and the condition on δ_0 (here $\delta_0 = \pi/2$). This is the reason why all the trajectories used in figures 2–5 to verify the analytical calculations developed in the present paper have initial values $\theta_0 = \pi/4$ and $\psi_0 = 0$.

The observed and calculated action integrals I' and $\mathcal{I}_2'$ against the initial value I_0 are plotted in figure 4. The calculated values are obtained from equations (4.5), (4.6) and (5.1). The 'observed' values for trajectories outside coupling-induced resonance islands (rotational trajectories) are obtained by measuring area in Poincaré surfaces of section (SOS), according to

$$I' = \frac{1}{2\pi G}(n'S_{I,\theta} + m'S_{J,\psi}) \qquad |\mathcal{I}_2'| = \frac{m'n'}{2\pi G}S_{I,\theta} \tag{5.2}$$

where $S_{I,\theta}$ denotes the area below the $I = I(\theta)$ curve in the first SOS (for θ varying from 0 to 2π) and $S_{J,\psi}$ the area below the $J = J(\psi)$ curve in the other SOS (be careful that ψ only varies from 0 to π [9]). Equation (5.2) is true at $K_C = 0$ and remains valid as long as I_0 does not cross one of the two values associated with the separatrices between trajectories inside and outside resonance islands ($I_0 \approx 14.121\,460$ and $I_0 \approx 14.426\,635$). This crossing causes a drastic change in the topology of the tori which support the trajectories and invalidates equation (5.2). It is seen that the agreement is excellent between observed and calculated action integrals. It is also noticed that for rotational trajectories, $\mathcal{I}_2'$ is very close to its asymptotic value for vanishing K_C, that is $\pm m'n'I_0/G$. As for the second action integral $\mathcal{I}_2$ of H_F, $\mathcal{I}_2'$ is discontinuous when I_0 crosses a separatix. Exact numerical calculation of action integrals inside coupling-induced resonance islands is not easily achievable, since one no longer knows the topology of the torus, which becomes very long and thin. The discontinuous deformation of tori at separatrices invalidates most general methods, as is acknowledged in [41]. It was, however, observed that the computed value of the area of the resonance island in the (I, θ) SOS divided by 2π is very close to the calculated value of $\mathcal{I}_2'$ (see the central part of the bottom figure in figure 4), which suggests that $\mathcal{I}_2'$ can be calculated exactly using (I, θ) Poincaré SOS. This point, which is not clearly understood, merits further investigation.

The observed and calculated frequencies $\nu^{*\prime}$ and $\omega^{*\prime}$ against the initial value I_0 are plotted in figure 5. The calculated values are obtained from equations (4.5) and (4.6). The 'observed' values, for trajectories both inside and outside coupling-induced resonance

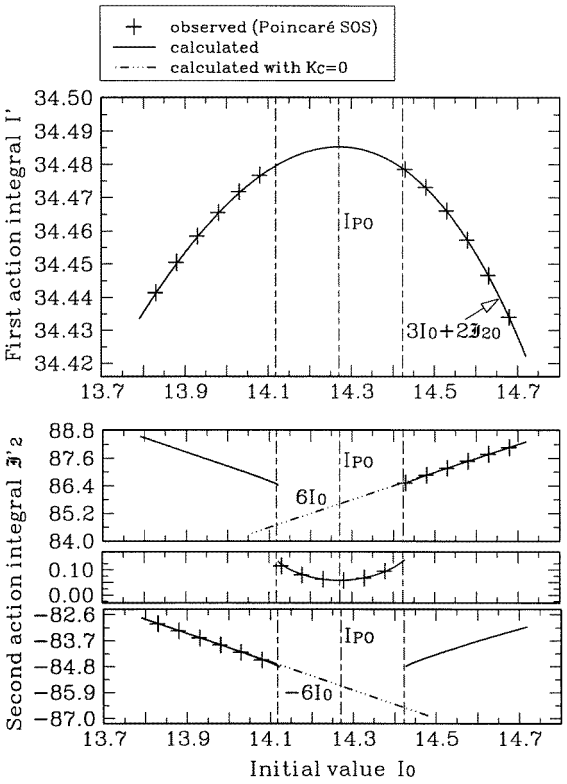

Figure 4. Plot of the action integrals I' and $\mathcal{I}_2'$ for initial values of I ranging from $I_0 = 13.83$ to $I_0 = 14.68$ (that is, surrounding the value $I_{PO} \approx 14.270\,25$ of the first action integral of the $\frac{2}{3}$ PO of H_F) for the non-integrable Hamiltonian H at energy $E = 15$. Other initial values are $\psi_0 = 0$ and $\theta_0 = \pi/4$ (see text). In both plots, the full curves represent the action integrals calculated according to the formulae in equations (4.5), (4.6) and (5.1). The dot-dashed line in the bottom plot corresponds to the limiting value of $\mathcal{I}_2'$ for vanishing values of K_C, that is $\pm 6I_0$. The exact values of the action integrals (+) are deduced from Poincaré SOS obtained by numerical integration of trajectories (see section 5).

islands, are deduced from the power spectra of the coordinate J obtained from numerical integration of Hamilton's equations: one actually just needs to follow the evolution (as a function of I_0) of the peaks, which far from the m'/n' PO of H_F appear very close to the frequencies ω^* and $m'\nu^* - n'\omega^*$. Indeed, according to section 4, $\nu^{*\prime}$ and $\omega^{*\prime}$ behave continuously when crossing separatrices and, in addition, for rotational trajectories the asymptotic values (both far from the PO or for vanishing values of K_C) of $\nu^{*\prime}$ and $\omega^{*\prime}$ are

$$\nu^{*\prime} \approx \frac{G}{m'}\omega^* \qquad \omega^{*\prime} \approx \frac{G}{m'}|m'\nu^* - n'\omega^*|. \tag{5.3}$$

The peak at ω^* is the strongest one in the power spectrum, whereas the peak at $m'\nu^* - n'\omega^*$ is very weak and grows nearly linearly with K_C. It is observed that the agreement is again excellent between observed and calculated frequencies. It is also noticed that, because of the vertical tangents at the separatices, the classical frequencies for non-resonant trajectories do not remain as close to their asymptotic values for vanishing values of K_C as the second action integral $\mathcal{I}_2'$ does. The perturbation on frequencies extends over a range of I_0, which is

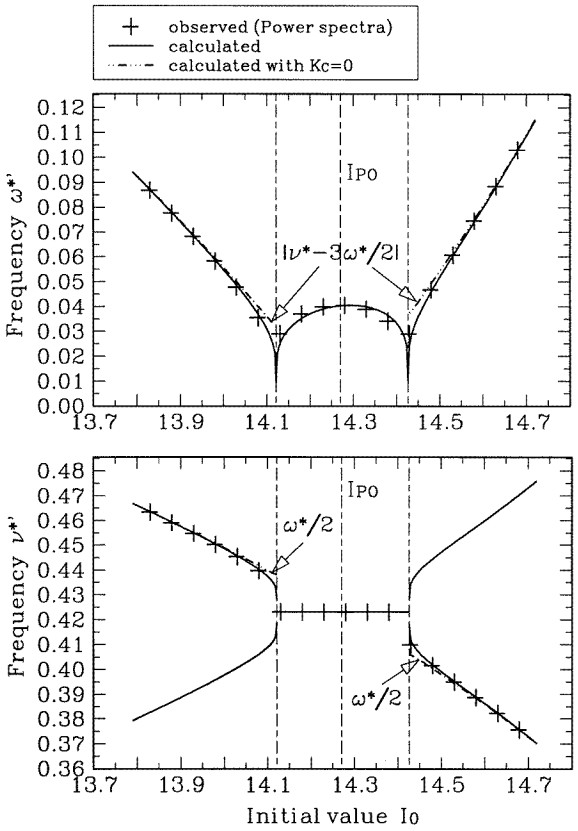

Figure 5. Plot of the classical frequencies $\omega^{*\prime}$ and $\nu^{*\prime}$ for initial values of I ranging from $I_0 = 13.83$ to $I_0 = 14.68$ (that is, surrounding the value $I_{\mathrm{PO}} \approx 14.270\,25$ of the first action integral of the $\frac{2}{3}$ PO H_{F}) for the non-integrable Hamiltonian H at energy $E = 15$. Other initial values are $\psi_0 = 0$ and $\theta_0 = \pi/4$ (see text). The dot-dashed line corresponds to combinations of the classical frequencies of H_{F} calculated using the formula in [17, 26] and equation (5.3) and the full curve to the frequencies of H calculated according to equations (4.5) and (4.6). The exact classical frequencies for the non-integrable Hamiltonian H are deduced from power spectra obtained from numerical integration of trajectories for a time $\Delta t = 30\,000$. The absolute precision for observed classical frequencies is about 10^{-4}.

roughly twice the range of I_0 for resonant trajectories. The most striking feature in figure 5 (as well as in figure 3) is the fact that one frequency remains mostly constant throughout the coupling-induced resonance island: simple Taylor expansions in equation (4.5) actually show that *all the trajectories inside coupling-induced resonance islands share an almost degenerate frequency* $\nu^{*\prime} \approx G\omega^*_{\mathrm{PO}}/m'$, where ω^*_{PO} denotes the second classical frequency of H_{F} at the PO. This property does not depend on the smallness of K_{C} (it was verified that it is still observed for values of K_{C} larger than the anharmonicity parameters) and seems to be a quite general phenomenon, since it is also noticeable in the study of Laskar dealing with the standard map [42]. On the other hand, reverting equation (5.3) enables the calculation of the frequencies ν^* and ω^* in figure 3. The discontinuity of ν^* at I_{PO} is just due to the sign change at I_{PO} of the term inside the absolute value in equation (5.3).

Another point, which is worth noting, deals with the width of the coupling-induced resonance islands. Indeed, Taylor expansions in equation (4.4) show that separatrices

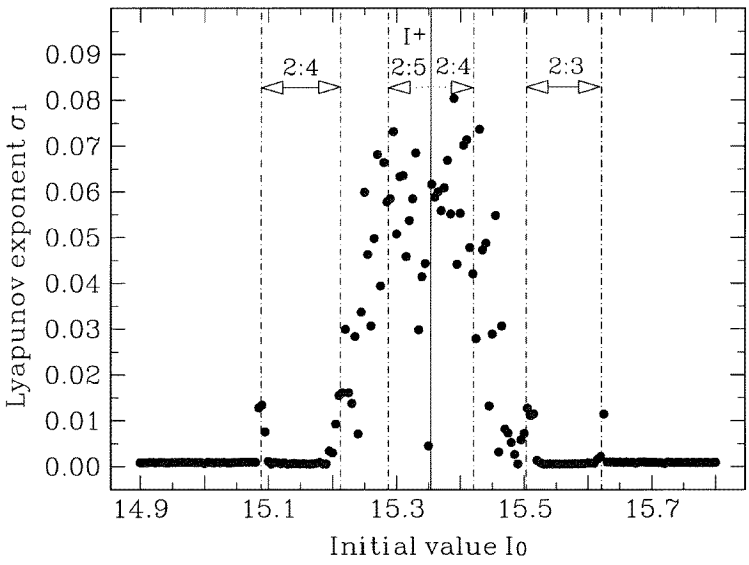

Figure 6. Plot of the maximal Lyapunov exponent σ_1 for trajectories of H with energy $E = 15$ and initial values $\theta_0 = \pi/4$, $\psi_0 = 0$ and I_0 ranging from 14.9 to 15.8. The positions of the separatrix I^+ of H_F, as well as the separatrices for the coupling-induced resonance islands, are indicated on the plot.

($A = B$, that is, $R = 1$) are approximately located at

$$I_0 \approx I_{PO} \mp \left(\left| \frac{2K'}{\omega^*_{PO}(\partial(\nu^*/\omega^*)/\partial I)_{PO}} \right| \right)^{1/2} \tag{5.4}$$

where the classical frequencies and their derivatives are calculated at I_{PO} and for $K_C = 0$. The expression in equation (5.4) leads to values of I_0 at the separatrices equal to $I_0 \approx 14.1178$ and $I_0 \approx 14.4228$, close to the exact values at $I_0 \approx 14.1215$ and $I_0 \approx 14.4266$. Equation (5.4) shows that the width of the coupling-induced resonance island grows as the square root of the perturbation parameter k_C, but is inversely proportional to the square root of the frequency ω^* of the periodic orbit and to the square root of the derivative with respect to I of the winding number ν^*/ω^*.

It can also be mentioned that this study provides a nice illustration of the criterion of overlapping resonances introduced by Chririkov in the 1950's [43] and further discussed by Walker and Ford [27] and Atkin and Logan [28, 29] (an actually much clearer illustration than a previous paper of mine on this subject, see [44]). This criterion states that widespread chaos occurs where coupling-induced resonance islands overlap. For the Hamiltonian in equations (2.5) and (2.6), it is seen using equation (4.4), that:

- below the separatrix of H_F at $I^+ \approx 15.353\,599$ [17, 26], all the $2/n'$ POs overlap for values of n' equal to or larger than five ($I_0 \geqslant 15.286\,77$), whereas the $\frac{2}{4}$ ($15.088\,97 \leqslant I_0 \leqslant 15.212\,25$) and $\frac{2}{3}$ ($14.121\,46 \leqslant I_0 \leqslant 14.426\,63$) POs remain well separated.
- above I^+, all the $2/n'$ POs overlap for values of n' equal to or larger than four ($I_0 \leqslant 15.420\,68$), whereas the $\frac{2}{3}$ ($15.503\,49 \leqslant I_0 \leqslant 15.621\,07$) and $\frac{2}{2}$ ($16.378\,24 \leqslant I_0 \leqslant 16.507\,21$) POs remain well separated.

(Due to the expression of H_C in equation (2.6), the procedure for the derivation of the local single resonance form of H in section 3 shows that only $2/n'$ resonance islands are expected to develop substantially.) Maximal Lyapunov exponents obtained using the

rescaling procedure described in [45] are drawn in figure 6 for values of I_0 ranging from 14.9 to 15.8. It is clearly seen in this figure that, in agreement with the criterion of Walker and Ford, the region of overlapping resonances is completely chaotic. However, the chaotic region extends somewhat further, and is actually stopped by the first well separated coupling-induced resonance islands which are encountered ($\frac{2}{4}$ islands below I^+ and $\frac{2}{3}$ islands above I^+).

6. Conclusion

In this paper, a study of the classical dynamics of a non-integrable Hamiltonian in the neighbourhood of coupling-induced resonance islands is performed. This study is both *statistical* and *iterative*. It is *statistical*, in the sense that it neglects higher-order small details. Indeed, the global features of the SOS in figure 1 can again be observed at a smaller scale around each set of coupling-induced resonance islands: in figure 6, thin regions of chaos are clearly seen around the separatrices of first-order, coupling-induced resonance islands. Similarly, the plot of SOS with a smaller increment of I_0 reveals very small, second-order, coupling-induced resonance islands around POs of the local single resonance form of the Hamiltonian H in equation (3.4) that is for low-order rational values of $\omega^{*\prime}/\nu^{*\prime}$, and so on for increasing detail orders. None of these details is reproduced by the perturbation method used in the discussion above. However, the procedure described in this article is also *iterative*, in the sense that second-order thin features can be taken into account along the same lines as first-order coupling induced resonance islands. That is, by (i) expanding the Hamiltonian H in equation (3.4) in terms of the I' and $\mathcal{I}_2'$ action integrals and (ii) Fourier expanding H_C in terms of the angles $\nu^{*\prime}t$ and $\omega^{*\prime}t$ conjugate to I' and $\mathcal{I}_2'$ and retaining only the almost secular term. The intricate route towards chaos of the 'double resonance' Hamiltonian in equation (2.2) can therefore, at least in part, be modelled.

References

[1] Delon A and Jost R 1991 *J. Chem. Phys.* **95** 5686
[2] Lafferty W J and Sams R L 1977 *J. Mol. Spectrosc.* **66** 478
[3] Bist H D and Brand J C D 1976 *J. Mol. Spectrosc.* **62** 60
[4] Yamanouchi K, Takeuchi S and Tsuchiya S 1990 *J. Chem. Phys.* **92** 4044
[5] Birkhoff G D 1966 *Dynamical Systems* vol 9 (New York: AMS Colloquium)
[6] Gustavson F G 1966 *Astron. J.* **71** 670
[7] Swimm R T and Delos J B 1979 *J. Chem. Phys.* **71** 1706
[8] Uzer T, Noid D W and Marcus R A 1983 *J. Chem. Phys.* **79** 4412
[9] Joyeux M 1996 *J. Mol. Spectrosc.* **175** 262
[10] Pique J P, Joyeux M, Manners J and Sitja G 1991 *J. Chem. Phys.* **95** 8744
[11] Bernath P F, Dulick M, Field R W and Hardwick J L 1981 *J. Mol. Spectrosc.* **86** 275
[12] Vasudev R 1982 *Chem. Phys.* **64** 167
[13] Sibert E L, Reinhardt W P and Hynes J T 1982 *J. Chem. Phys.* **77** 3583
[14] Sibert E L, Hynes J T and Reinhardt W P 1982 *J. Chem. Phys.* **77** 3595
[15] Kellman M E 1985 *J. Chem. Phys.* **83** 3843
[16] Li Z, Xiao L and Kellman M E 1990 *J. Chem. Phys.* **92** 2251
[17] Joyeux M 1994 *Chem. Phys.* **185** 263
[18] Uzer T and Marcus R A 1984 *J. Chem. Phys.* **81** 5013
[19] Martens C C and Ezra G S 1987 *J. Chem. Phys.* **86** 279
[20] Xiao L and Kellman M E 1989 *J. Chem. Phys.* **90** 6086
[21] Joyeux M 1995 *J. Chem. Phys.* **102** 2816
[22] Stuchebrukhov A A and Marcus R A 1993 *J. Chem. Phys.* **98** 8443
[23] Ramachandran B and Kay K G 1993 *J. Chem. Phys.* **99** 3659

[24] Rouben D C and Ezra G S 1995 *J. Chem. Phys.* **103** 1375
[25] Joyeux M 1995 *Chem. Phys. Lett.* **247** 454
[26] Joyeux M 1996 *Chem. Phys.* **203** 281
[27] Walker G H and Ford J 1969 *Phys. Rev.* **188** 416
[28] Atkins K M and Logan D E 1992 *J. Chem. Phys.* **97** 2438
[29] Atkins K M and Logan D E 1992 *Phys. Lett.* **162A** 255
[30] Talanina I B and Collins M A 1993 *J. Chem. Phys.* **98** 1817
[31] Joyeux M 1992 *Chem. Phys.* **167** 299
[32] Kolmogorov A N 1954 *Dokl. Akad. Nauk. SSSR* **98** 525
[33] Kolmogorov A N 1957 *Proc. of the 1954 Int. Congress of Mathematics* (Amsterdam: North-Holland)
[34] Moser J 1962 *Nachr. Akad. Wiss. Goettingen Math. Phys.* **K1** 1
[35] Arnold V I 1963 *Russ. Math. Surv.* **18** 85
[36] Tabor M 1989 *Chaos and Integrability in Nonlinear Dynamics* (New York: Wiley)
[37] Ozorio de Almeida A M 1986 *Lect. Notes Phys.* **263** 197
[38] Tomsovic S, Grinberg M and Ullmo D 1995 *Phys. Rev. Lett.* **75** 4346
[39] Fröman S 1979 *J. Phys. A: Math. Gen.* **12** 2355
[40] Connor J N L, Uzer T, Marcus R A and Smith A D 1984 *J. Chem. Phys.* **80** 5095
[41] Percival I C and Pomphrey N 1976 *Mol. Phys.* **31** 97
[42] Laskar J 1994 *Workshop on Non-Linear Dynamics in Particle Accelerators (Arcidosso, 1994)*
[43] Chirikov B 1979 *Phys. Rep.* **52** 263
[44] Joyeux M 1993 *Chem. Phys.* **174** 157
[45] Benettin G, Galgani K and Strelcyn J M 1976 *Phys. Rev.* A **14** 2338